1
2
3
4
5
6
7
8
9
10
11
12
13
14
15
16
17
18
19
20
21
22
23
24
25
26
27
28
29
30
31
32
33
34
35
36
37
38
39
40
41
42
43
44
45
46
47
48
49
50
51
52
53
54
55
56
57
58
59
60

A photoluminescence study of CuInSe$_2$ single crystals ion implanted with 5 keV hydrogen

M.V. Yakushev,[1,2,3] J.Krustok,[4] M. Grossberg,[4] V.A. Volkov,[2] A.V. Mudryi[5] and R.W. Martin[1]

[1] Department of Physics, SUPA, Strathclyde University, G4 0NG Glasgow, UK

[2] Ural Federal University, Ekaterinburg, 620002, Russia

[3] Institute of Solid State Chemistry of RAS, Ekaterinburg, 620990, Russia

[4] Department of Materials Science, Tallinn University of Technology, 19086 Tallinn, Estonia

[5] Scientific-Practical Material Research Centre of National Academy of Science of

Belarus, 220072 Minsk, Belarus

E-mail: michael.yakushev@strath.ac.uk

Abstract

$CuInSe_2$ single crystals ion implanted with 5 keV hydrogen at doses from $3x10^{14}$ to 10^{16} cm^{-2} are studied by photoluminescence (PL). The PL spectra before and after implantation reveal two bands, a main dominant band centred at 0.96 eV and a lower intensity band centred at 0.93 eV. Detailed analysis of the shape of these bands, their temperature and excitation intensity dependencies allow the recombination mechanisms to be identified as band-to-tail (BT) and band-to-impurity (BI), respectively. The implantation causes gradual red shifts of the bands increasing linearly with the dose. The average depth of potential fluctuations is also estimated to increase with the dose and saturates for doses above 10^{15} cm^{-2}. A model is proposed which associates the potential fluctuations with the antisite defects copper on indium site and indium on copper site. The saturation is explained by full randomisation of copper and indium atoms on the cation sub-lattice.

Keywords: $CuInSe_2$, Ion-implantation, Photoluminescence

1. Introduction

The semiconductor compound $CuInSe_2$ is used in the absorber layer of solar cells which are amongst the leaders for thin film photovoltaic (PV) devices [1]. The record conversion efficiency for a laboratory size solar cell using $Cu(In,Ga)Se_2$ absorber, where $CuInSe_2$ is alloyed with $CuGaSe_2$ to optimise the bandgap, exceeds 21% [2].

One of the intriguing properties of such cells is their high stability under radiation. Early measurements of the principal solar cell parameters for $CuInSe_2$ absorber layer, without gallium, demonstrated that their tolerance to MeV proton radiation is at least 50 times higher than that of Si- and GaAs - based devices [3]. Subsequently it was shown that $Cu(InGa)Se_2$ - based devices are

at least as radiation hard against 3 MeV proton radiation as InP/Si cells specifically designed for space applications [4]. Such a radiation tolerance of the solar cells has been associated with the radiation hardness of the basic material $CuInSe_2$ itself. Raman studies of $CuInSe_2$ single crystals implanted at room temperature with a variety of ions showed a very high tolerance of their lattice structure against radiation damage. This was explained by an efficient defect healing mechanism, which facilitates the recombination of the majority of primary defects, vacancies and interstitials, generated in collision processes during or shortly after the implantation [5]. The extraordinary radiation hardness of $CuInSe_2$ and of solar cells based on this material suggests a potential for the use of such devices in spacecraft power generators [3,4,5].

Photoluminescence (PL) is one of the most efficient techniques to analyse the electronic properties of defects in semiconductors [6]. PL studies of $Cu(In,Ga)Se_2$ thin films implanted with 2.5 keV protons demonstrated that at lower doses the intensity of the main PL emission band, present before implantation, increases whereas its spectral position shifts towards higher energies [7]. Such changes were interpreted as beneficial for the electronic properties and attributed to the passivation effect of hydrogen atoms filling copper vacancies which are considered to be the main p-type doping defects. Higher doses of protons attenuated the intensity of the main PL band and shifted the band spectral position to lower energies. The implantation also induced three new deeper bands. Similar deep bands were also observed after implantation of protons at energies of 200 keV [8] and 380 keV [9] into $Cu(In,Ga)Se_2$ solar cells and thin films, respectively. Deep bands were also observed after irradiation with deuterium and helium ions suggesting that such bands are likely to be associated with collision induced defects rather than chemical effects of hydrogen [10].

However very little can be found in the literature on the effects of ion implantation on the PL spectra of $CuInSe_2$ single crystals. A PL study of $CuInSe_2$ single crystals ion implanted with Xe^+, Ar^+ and Ne^+ provided limited information on the physical nature of the defects generated by radiation and the mechanisms underlying the radiation hardness of $CuInSe_2$ [11]. Before

irradiation the PL spectra were dominated by a broad and asymmetric band with a maximum at 0.92 eV, typical for $CuInSe_2$. The irradiation did not induce any new features in the PL spectral within the measured region from 900 to 1700 nm but caused gradual attenuations of the band intensity with increasing dose. This was attributed to an increasing populations of non-radiative traps.

In this paper we present a PL study of a $CuInSe_2$ single crystal ion implanted with 5 keV hydrogen at doses from 3×10^{14} to 10^{16} cm^{-2}. The PL spectra revealed a main dominant BT band centred at 0.96 eV and a lower intensity band centred at 0.93 eV. Detailed analysis of the shape of these bands, their temperature and excitation intensity dependencies helped to identify their recombination mechanisms as band-to-tail (BT) and band-to-impurity (BI). Increasing implantation doses cause red shifts of the bands. The estimated average depth of potential fluctuations increases with the dose and saturated at higher values.

2. Experimental details

The *p*-type conducting sample originating from the middle part of a $CuInSe_2$ single crystal grown by the vertical Bridgman technique from a near stoichiometric charge of pure elements [12]. It was cut perpendicular to the growth direction and has dimensions 16x7 mm^2, and a thickness of 2 mm. One surface of the sample was mechanically polished with different grades of diamond paste (from 5 to 1 μm) and in a vibrating water bath with 0.05 μm Al_2O_3 powder. The polished sample was etched in 5% bromine-methanol solution and then annealed at 300° C in vacuum following a surface preparation procedure, developed for Rutherford Backscattering/channelling and Raman analysis of $CuInSe_2$ [13]. The elemental composition of the sample, measured using energy dispersive x-ray analysis, was found to be close to the ideal stoichiometry Cu:25.3, In:25.5 and Se:49.2 at.%.

The prepared surface was ion implanted at room temperature with 3×10^{14}, 10^{15}, 3×10^{15} and 10^{16} cm^{-2} doses of 5 keV H$^+$ in 3 mm wide stripes leaving some surface areas screened from the irradiation for reference.

The sample was studied by PL at temperatures from 20K to 150K achieved by cooling in an optical closed cycle helium refrigerator. The 514 nm line of a 100 mW Ar$^+$ laser was used for excitation. Detection employed a liquid-nitrogen cooled Ge p-i-n diode.

3. Results and discussion

The normalised PL spectra of the sample measured at 20 K in the non-implanted and implanted areas are shown in Fig.1. The spectra in both the non-implanted and implanted areas are dominated by a broad and asymmetrical band BT, denoting band-to-tail, with its maximum near 0.96 eV. The shape of this band, dropping steeply on the higher energy side and with a tail on the low energy side, is characteristic of transitions involving band tails [14] induced by spatial potential fluctuations present due to a high concentration of randomly distributed charged defects [15].

The spectra also reveal a BI-band, which denotes band-to-impurity, at about 0.93 eV. This band can be seen resolved in the spectra of non-implanted material whereas in the implanted areas its intensity is lower and it merges with the BT band. The intensity of the BT and BI bands was found to change across the implanted and non-implanted areas whereas their spectral positions remain unchanged, suggesting a non-homogeneity of the elemental composition across the sample surface. Therefore changes in the band intensity are not used to analyse effects of the implantation.

Fig.1 shows that implantation of hydrogen shifts the BT band to lower energies, with the shift increasing linearly with the dose. The implantation does not create any new band in the PL spectra within the studied spectral region.

Excitation intensity and temperature dependencies of the spectra were measured to identify the origin of these bands.

A typical example of the dependency of the PL spectra on the excitation intensity in the material implanted with a dose of 10^{15} cm^{-2} is shown in Fig.2. It can be seen that increasing laser power shifts both the BT and BI band towards higher energy. The rates of such shifts are j(BT) = (14 ± 1) meV and j(BI) = (12 ± 1) meV per decade of power change for the non-implanted material. These match those for the implanted material, within the error corridor, indicating that ion implantation does not change the j-shifts. Blue shifts of PL bands at increasing excitation intensity are often interpreted as identification of a donor – acceptor pair (DAP) mechanism: a recombination of acceptor localised hole and donor localised electron. However, the rate of such a j- shift for such a recombination should not exceed a few meV per decade. The larger j-shifts, observed for both the BT and BI bands and their asymmetric shape at low temperatures are characteristics of band tail related recombination mechanisms [14].

Rising temperature quenches the intensity of the PL emission. Fig.3(a) shows a typical example of the temperature dependency of the PL spectra in the area implanted with a dose of 10^{15} cm^{-2}. The BI band quenches by 40 K whereas the BT band has a significant intensity at 110 K red shifting up to 70 K and then blue shifting at higher temperatures. The shape of the spectra and the shifts are seen more clearly in Fig.3(b) where these spectra are normalised, offset and shown on a linear scale. Such red shifts at increasing temperature are another indication of the involvement of band tails in the recombination mechanisms of the bands [14]. For the laser powers used in these experiments and with the Ge detector, the PL emission is fully quenched at about 200 K.

A semiconductor is highly doped if the average distance between its defects is smaller than their Bohr radii, causing the wave-functions of these defects to overlap [15]. The condition of high doping for donors and acceptors are different if the effective masses of the electron m^*_e and hole m^*_h are significantly different. In CuInSe$_2$ the density of states hole mass $m^*_h=0.71m_e$

[16] is significantly greater than that of electron m^*_h=0.09m_e [17]. CuInSe$_2$ contains both donors and acceptors showing p-type conductivity if the concentration of acceptors is higher than that of donors. Because its electrons are lighter than holes the high doping condition is usually achieved for donors but not achieved for acceptors [18].

According to the theory of highly doped semiconductors with spatial potential fluctuations [14,18] low temperature radiative recombination can originate from the recombination of free electrons from the quasi-Fermi level for electrons F_n with holes, localised in the valence band tail (BT band) or holes localised at an acceptor state (BI-band) deep enough not to overlap with the valence band tail. Energy diagrams of the BT and BI transitions are shown in Fig.4(a). The figure also shows the density of states for the conduction ρ_c and valence ρ_v bands as well as that of an acceptor level ρ_a participating in the BI transition in a semiconductor with spatial potential fluctuations.

At low temperature holes are captured at deep states in the valence band tail acting like acceptor levels [14]. The average amplitude of potential fluctuations γ determines the spectral position of the bands in the PL spectra and the value of their j-shifts. The higher the average amplitude of the potential fluctuations the greater is the j-shift and the smaller is the spectral energy of the BT band. Thus the BT band red-shifts with increasing dose, as this increases γ. Spatial potential fluctuations also influence the spectral energy of the BI band by changing the material bandgap.

The BI-band quenches quickly at increasing temperature and it is difficult therefore to carry out detailed analysis of its temperature dependencies. However its spectral position, j-shift and shape indicate that it originates from the band-to-impurity recombination mechanism.

According to ref. [14] the spectral position of the BT- band maximum $h\nu_{max}$(BT) can be described as:

$$h\nu_{max}(BT) = h\nu^0_{max} - kT \ln[N_v/(p+\theta n)], \tag{1}$$

Where N_v is the effective density of states in the valence band, n and p are concentrations of free electrons and holes, respectively, θ is the ratio of electron to hole probabilities to be captured by the localised state. At low temperatures and low excitation intensities an increase in temperature results in a red shift of the BT band. Once the temperature becomes higher than T_1, a characteristic value for the BT transition, hv_{max}(BT) starts shifting blue because the holes, localised at the states of the valence band tails, thermalise to the valence band. At T_1 hv_{max}(BT) has its minimum value. Such a temperature dependence of hv_{max}(BT) red-shifting up to a temperature of 70 K and then blue-shifting at higher temperatures can be seen in Fig.3(b) and Fig.4(b).

Both the minimum value of hv_{max}(BT) and T_1 depend on the carrier concentration which depends on the excitation intensity. Higher excitation intensities shift hv_{max}(BT) towards higher energies because of increasing n and p. Smaller carrier concentrations correspond to lower values of hv_{max}(BT) as shown in Fig.4(b) where T_1 is decreasing from 67 to 53 K for excitation laser power increasing from 3 to 30 mW.

The low-energy side of the BT-band is defined by the valence band tail density of states and depends neither on temperature nor on excitation intensity. It can be described by the following expression $I_{LE} \propto \exp\{-(E_g - hv)/\gamma\}$ [14,18]. The excitation intensity and temperature dependencies of the BT band shown in Fig.2 and 3 clearly demonstrate this. The shape of the high-energy side has a more complex nature.

In materials with spatial potential fluctuations the BI band also shows a characteristic asymmetric shape, a red shift with increasing temperature and a significant blue shift with increasing excitation intensity [17,19]. BI includes two processes: BI_1, the recombination of free holes captured at the acceptors, and BI_2, the recombination of holes first captured at the valence band tail states, as shown in Fig.4(a). Therefore similar to the BT band the valence band tail density of states also determines the shape of the low energy side of the BI band [19].

8

The shape of the low energy side of the BT and BI bands can be used to estimate γ. To determine γ and improve the accuracy of the analysis the experimental spectra were fitted with the empirical double sigmoidal function proposed in ref. [18]:

$$I(h\nu) = A(1/(1+\exp[-(h\nu-E_1)/W_1]))(1-1/(1+\exp[-(h\nu-E_2)/W_2])), \tag{2}$$

where A, $E1$, $E2$, $W1$ and $W2$ are the fitting parameters, $E1$ and $W1$ represent the low-energy side of the PL band whereas $E2$ and $W2$ are responsible for the high-energy side. An example of such fit for the BT and BI bands in the PL spectrum of $CuInSe_2$ implanted with 10^{15} cm^{-2} of H^+ is shown in Fig.5(a). Such fitting allows a better estimate of the spectral position of the BI band in spectra where the BI and BT are not well resolved. The dependencies of the spectral position of these bands on the implantation dose are shown in Fig.5(b). The BT band red shifts at a rate of 2.5 meV per decade of implantation dose whereas the BI band shift rate of 0.1 meV per decade is significantly smaller.

The estimated values of γ for non–implanted $CuInSe_2$ and the dependence of γ on the implantation dose are plotted in Fig.6. A significant increase in the average depth of potential fluctuation can be seen after the implantation with doses up to 10^{15} cm^{-2} whereas implantation with higher doses results in a saturation of the growth of γ. For low doses of hydrogen we observe no blue shifts of the BT band similar to those reported for $Cu(In,Ga)Se_2$ thin films ion implanted with 2.5 keV hydrogen [23]. This can be explained by the higher energy of the implanted hydrogen. According to TRIM simulations [24] one 5 keV proton generates 5 vacancies whereas one 2.5 keV proton produces only 2.5 vacancies per ion.

Protons generate primary displacement defects, vacancies and interstitials in the lattice of $CuInSe_2$. According to TRIM simulations 5 keV protons create a 54 nm thick layer of primary defects at an average depth of 38 nm. At room temperature however primary structural defects are known to be unstable and interact with each other and with the crystalline lattice to form

9

more stable defect complexes. The radiation damage produced by 10 keV protons implanted in CuInSe$_2$ single crystal with a dose of 3×10^{16} cm^{-2} has been studied by Rutherford backscattering-channelling [25]. The experimentally estimated concentration of atoms in the indium sub-lattice displaced to interstitial positions was found to be less than 20% of that predicted by TRIM one suggesting that more than 80% of primary defects are healed during or shortly after the implantation. The energy required to create a structural defect can be presented as the sum of two terms: energy for the structural change and electronic energy [26]. The latter depends on the position of the defect level within the bandgap with respect to the Fermi level. The electronic energy influences whether the formed secondary defects are *n* or *p*-type favouring the formation of deep compensating states. Therefore after the 5 keV implantation in CuInSe$_2$ we can expect the formation of secondary defects with energy levels located deep in the bandgap. Their accumulation is responsible for the observed growth of the average amplitude of potential fluctuations with the dose of implantation. Such defects are likely to contain hydrogen. According to TRIM simulations 5 keV protons are distributed within a 48 nm thick layer at an average depth of 56 nm. After a dose of 10^{15} cm^{-2} the maximum concentration of hydrogen is estimated to be about 0.5% and after a dose of 10^{16} cm^{-2} about 5% of the atomic density of CuInSe$_2$. Measurements of depth concentrations profiles of 10 keV hydrogen, ion implanted in CuInSe$_2$ single crystals, using the ^{1}H(^{15}N,$\alpha\gamma$)^{12}C nuclear reaction method showed that some hydrogen atoms stay trapped in the layer of implantation whereas a significant fraction of it diffuses deeper [27].

Positron annihilation measurements of CuInSe$_2$ single crystals, irradiated with a dose of 10^{18} cm^{-2} of 2 MeV electrons, suggested the formation of antisite-type defects as probable candidates for secondary radiation defects at room temperature whereas high concentrations of vacancy like defects should not be expected [28]. According to *ab-initio* calculations [29] in CuInSe$_2$ at near stoichiometric compositions, leading candidates for such antisite defects can be bare copper on indium site Cu$_{In}$ and indium on the copper site In$_{Cu}$. Ordered positions of copper and indium on the

cation sublattice results in the chalcopyrite structure whereas their randomisation is a characteristic of sphalerite structure. Because the sphalerite to chalcopyrite phase transition takes place at a temperature below the melting point [12] the cation sublattice always has a degree of randomisation. Cu_{In} antisites with a concentration of $3 \cdot 10^{20}$ cm^{-3} were found using neutron scattering in non-irradiated $CuInSe_2$ [30]. Thus high concentrations of the Cu_{In} and In_{Cu} antisites are likely to be present after the proton implantation.

The saturation in the growth of the average depth of potential fluctuation at doses of 10^{16} cm^{-2} can probably be attributed to the total randomisation of the cation sublattice transforming the chalcopyrite lattice to the sphalerite one. This is supported by TRIM simulations which show that after a dose of 10^{16} cm^{-2} of about 100% of lattice atoms should be knocked out of their lattice locations. Such a transformation has been observed after the bombardment of $CuInSe_2$ single crystals with 1.5 keV Ar ions [31].

4. Conclusion

$CuInSe_2$ single crystals ion implanted with doses from 3×10^{14} to 10^{16} cm^{-2} of 5 keV hydrogen were studied by photoluminescence. The PL spectra measured before and after the implantation reveal two bands: a main higher energy BT band dominating the spectra and a lower energy BI one. Detailed analysis of the band shape, their dependencies on temperature and excitation intensity provided evidences to identify their recombination mechanisms as band-to-tail (BT) and band-to-impurity (BI). Increasing implantation doses cause red shifts of the bands linearly dependent on the dose. The estimated average depth of potential fluctuations was found to increase with the dose and saturates at doses above 10^{15} cm^{-2}. A model connecting the potential fluctuations with the antisite defects copper on indium site and indium on copper site is proposed. The saturation is explained by full randomisation of copper and indium atoms on the cation sub-lattice.

Acknowlegments

References

[1] Green M A, Emery K, Hishikawa Y, Warta W, Dunlop E D 2015 Solar cell efficiency tables *Progress in Photovoltaics: Research and Applications* **23** 1 - 9

[2] Jackson P, Hariskos D, Wuerz R, Kiowski O, Bauer A T, Powalla M M 2015 Properties of $Cu(In,Ga)Se_2$ solar cells with new record efficiencies up to 21.7% *Physica Status Solidi - Rapid Research Letters* **9** 28 - 31

[3] Burgess R M, Chen W S, Devaney W E, Doyle D H, Kim N P, Stanbery B J 1988 Electron and proton radiation effects on GaAs and $CuInSe_2$ thin film solar cells, Proceedings of the 20th IEEE Photovoltaic Specialists Conference, IEEE. New York, USA 909-11

[4] Jasenek A and Rau U 2001Defect generation in $Cu(In,Ga)Se_2$ heterojunction solar cells by high-energy electron and proton irradiation *J. Appl. Phys.* **90** 650-8

[5] Lippold G, Yakushev M,Tomlinson R D, Hill A E, Grill W A 1996 Raman Scattering Study of Ion Implantation Damage in $CuInSe_2$ Single Crystals *Cryst. Res.Technol.* **31** 381-4

[6] Williams E W *and* Bebb H B 1972 *Semiconductors and Semimetals* **8** (R. K. Willardson and A. C. Beer, eds., New York: Academic Press)

[7] Yakushev M V, Martin R W, Urquhart F, Mudryi A V, Schock H W, Krustok J, Pilkington R D, Hill A E, Tomlinson R D 2000 A PL Study of Hydrogen Implanted Cu(InGa)Se$_2$ Thin Films *Jap. J. Appl. Phys.* **39-1** 320-23

[8] Hirose Y, Warasawa M, Tsunoda I, Takakura K, Sugiyama M 2012 Effects of Proton Irradiation on Optical and Electrical Properties of Cu(In,Ga)Se$_2$ Solar Cells *Jpn. J. Appl. Phys.* **51** 111802

[9] Mudryi A V, Ivanyukovich A V, Yakushev M V, Kulikauskas V S, Chernysh V S 2006 Defect formation in thin films of the semiconductor compound Cu(In,Ga)Se$_2$ when bombarded by protons *Journal of Applied Spectroscopy* **73** 928-31

[10] Yakushev M V, Martin R W, Krustok J, Schock H W, Pilkington R D, Hill A E, Tomlinson R D 2000 A PL Study of CIGS Thin Films Implanted With He and D Ions *Thin Solid Films* **361-362** 488-93

[11] Yakushev M, Urquhart F, Martin R W, Faunce C A, Hill A E, Pilkington R D, Tomlinson R D 1998 Photoluminescence Study of Radiation Damage in CuInSe$_2$ Single Crystals *Inst. Phys. Conf. Ser.* **152** 437-40

[12] Tomlinson R D 1986 Fabrication of CuInSe$_2$ Single Crystals Using Melt-Growth Technique *Solar Cells* **16** 17-26

[13] Yakushev M V, Lippold G, Hill A E, Pilkington R D, Tomlinson R D 1996 Rutherford Backscattering-channelling and Raman Study of CuInSe$_2$ Single Crystals surfaces *Journal of Material Science: Materials in Electronics* **7** 155-60

[14] Levanyuk A P, Osipov V V 1981 Edge luminescence of direct-gap semiconductors *Soviet Physics Uspekhi* **24** 187 - 215

[15] Shklovskii B I, Efros A L 1984 *Electronic properties of doped semiconductors* (Berlin: Springer-Verlag)

[16] Yakushev M V, Luckert F, Rodina A V, Faugeras C, Mudryi A V, Karotki A V and Martin R W 2012 Anisotropy of Effective Masses in CuInSe$_2$ *Appl. Phys. Lett.* **101** 262101

[17] Weinert H, Neumann H, Hobler H, Kuhn G, Nam N V 1977 *Phys. Status Solidi B* **81** K59-61

[18] Krustok J, Collan H, Yakushev M and Hjelt K 1999 The role of spatial potential fluctuations in the shape of the PL bands of multinary semiconductor compounds *Physica Scripta* **T79** 179-81

[19] Jagomagi A, Krustok J, Raudoja J, Grossberg M, Danilson M, Yakushev M 2003 Photoluminescence studies of heavily doped CuInTe$_2$ crystals *Physica B* **337** 369–74

[20] Bhattacharya R, Pal B, Bansal B 2012 On conversion of luminescence into absorption and the van Roosbroeck-Shockley relation *Appl. Phys. Lett.* **100** 222103

[21] Yakushev M V, Jones P A, Neumann H, Stephens G A, Tomlinson R D 1993 Ion Channelling Study of Hydrogen Induced Damage in CuInSe$_2$ Single Crystals *Nucl. Instr. Meth. Lett. B* **84** 405-7

[22] Yakushev M V, Neumann H, Tomlinson R D, Rimmer P, Lippold G 1994 Influence of Proton Implantation on the Properties of CuInSe$_2$ Single Crystals (II) *Cryst. Res. Technol.* **29** 417-26

[23] Yakushev M V, Martin R W, Urquhart F, Mudri A V, Schock H W, Krustok J, Pilkington R D, Hill A E, Tomlinson R D A 2000 PL Study of Hydrogen Implanted Cu(InGa)Se$_2$ Thin Films *Jap. J. Appl. Phys*. **39-1** 320-23

[24] Biersack J P, Haggmark L G 1980 Monte Carlo program for the transport of energetic ions in amorphous material *Nucl. Instr. Meth*. **174** 257-68

[25] Yakushev M V, Lippold G, Hill A E, Pilkington R D, Tomlinson R D 1995 An RBS-Channelling and Raman Study of Implant Damage in Hydrogen Implanted CuInSe$_2$ Single Crystals *Cryst. Res. Technol*. **95** 357-60

[26] Walukiewicz W 1988 Mechanisms of Fermi Level Stabilization in Semiconductors *Phys. Rev. B* **37** 4760-63

[27] Fink D, Krauser J, Lippold G, Yakushev M V,Tomlinson R D, Weidinger A, Dwivedi K K, Ghosh S, Chung W H 1998 On the Redistribution of 10keV Hydrogen in $CuInSe_2$ *Rad. Eff. Def. in Solids* **145** 85-105

[28] Polity A, Krause-Rehberg R, Staab T E M, Pushka M J, Klais J, Moller H J, Meyer B K 1998 Study of defects in electron irradiated $CuInSe_2$ by positron lifetime Spectroscopy *J. Appl. Phys.* **83** 71-8

[29] Zhang S B,. Wei S-H, Zunger A 1998 Defect physics of the $CuInSe_2$ chalcopyrite semiconductor *Phys. Rev. B* **57** 9642-56

[30] Stephan C, Schorr S, Tovar M and Schock H-W 2011 Comprehensive insights into point defect and cluster formation in $CuInSe_2$ *Appl. Phys. Lett.* **98** 091906

[31] Corvini P, Kahn A, Wagner S 1985 Surface order and stoichiometry of sputter-cleaned and annealed $CuInSe_2$ *J. Appl. Phys.* **57** 2967-9

Figure 1. Normalised PL spectra of $CuInSe_2$ single crystals before and after implantation of 5 keV hydrogen with different doses. The spectra are shifted along the y-axis for clarity.

Figure 2. Dependence of normalised PL spectra from the region of the $CuInSe_2$ crystal implanted with a dose of 10^{15} cm^{-2}, on excitation laser power. The spectra are shifted along the y-axis for clarity.

Figure 3. Temperature dependence of PL spectra from the region of the $CuInSe_2$ crystal implanted with a dose of 10^{15} cm^{-2} shown on a log scale (a), normalised temperature dependence shown on a linear scale and shifted along the y-axis for clarity (b).

Figure 4. Density of states for the conduction ρ_c and valence ρ_v bands as well as that of an acceptor level ρ_a in a semiconductor with potential fluctuations and energy diagram of band-to-tail (BT) and band-to-impurity (BI) recombination mechanisms shown by the dashed arrows (a); temperature dependencies of $h\nu_{max}$ of the BT band measured at different excitation intensities (b).

Figure 5. Fit of the PL spectrum of $CuInSe_2$ implanted with 10^{15} cm^{-2} by the empirical asymmetric double sigmoidal functions (a); Dependence of the spectral position of the BT and BI bands on the implantation dose (b).

Figure 6. Dependence of average amplitude of the potential fluctuations on implantation dose.

16

1
2
3
4
5
6
7
8
9
10
11
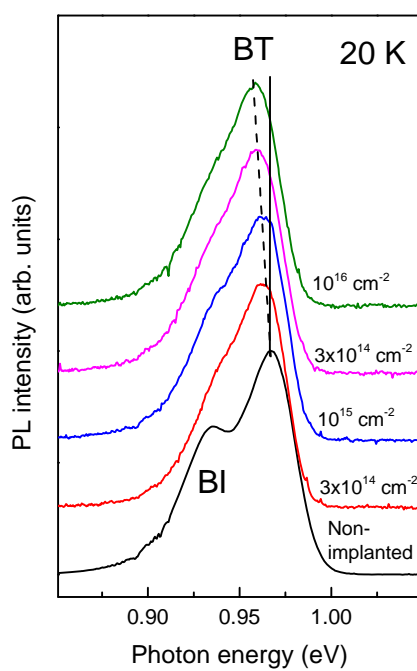12
13
14
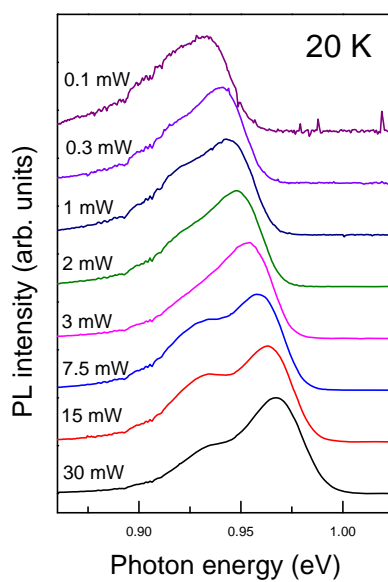15
16
17
18
19
20
21
22
23
24
25
26
27
28
29
30
31
32
33
34
35
36
37
38
39
40
41
42
43
44
45
46
47
48
49
50
51
52
53
54
55
56
57
58
59
60

Figure 1

Figure 2

1
2   Figure 3
3
4
5
6
7
8
9
10
11
12
13
14
15
16
17
18
19
20
21
22
23
24
25
26
27
28
29
30
31
32
33
34
35

36
37
38
39
40
41
42
43
44
45
46
47
48
49
50
51
52
53
54
55
56
57
58
59
60

1
2
3
4
5
6
7
8
9
10
11
12
13
14
15
16
17
18
19
20
21
22
23
24
25
26
27
28
29
30
31
32
33
34
35
36
37
38
39
40
41
42
43
44
45
46
47
48
49
50
51
52
53
54
55
56
57
58
59
60

Figure 4

1
2   Figure 5
3
4
5
6
7
8
9
10
11
12
13
14
15
16
17
18
19
20
21
22
23
24
25
26
27
28
29
30
31
32
33
34
35
36
37
38
39
40
41
42

43
44
45
46
47
48
49
50
51
52
53
54
55
56
57
58
59
60

1
2
3
4
5
6
7   Figure 6
8
9
10
11
12
13
14
15
16
17
18
19
20
21
22
23
24
25
26
27
28
29
30
31
32
33
34
35
36
37
38
39
40
41
42
43
44
45
46
47
48
49
50
51
52
53
54
55
56
57
58
59
60